CONFERENCE PRE-PRINT

TECHNOLOGIES OF HIGH VOLTAGE NEUTRAL BEAM INJECTORS FOR MAGNETIC FUSION DEVICES

O. Sotnikov

Budker Institute of Nuclear Physics SB RAS Novosibirsk, Russian Federation Email: O.Z.Sotnikov@inp.nsk.su

A. Sanin

Budker Institute of Nuclear Physics SB RAS Novosibirsk, Russian Federation Email: A.L.Sanin@inp.nsk.su

A. Belavsky

Budker Institute of Nuclear Physics SB RAS Novosibirsk, Russian Federation Email: A.V.Belavsky@inp.nsk.su

Yu. Belchenko

Budker Institute of Nuclear Physics SB RAS Novosibirsk, Russian Federation Email: Yu.I.Belchenko@inp.nsk.su

A. Gorbovsky

Budker Institute of Nuclear Physics SB RAS Novosibirsk, Russian Federation Email: A.I.Gorbovsky@inp.nsk.su

A. Gmyrya

Budker Institute of Nuclear Physics SB RAS Novosibirsk, Russian Federation Email: A.A.Gmyrya@inp.nsk.su

I. Emelev

Budker Institute of Nuclear Physics SB RAS Novosibirsk, Russian Federation Email: I.S.Emelev@inp.nsk.su

R. Finashin

Budker Institute of Nuclear Physics SB RAS Novosibirsk, Russian Federation Email: R.A.Finashin@inp.nsk.su

A. Kondakov

Budker Institute of Nuclear Physics SB RAS Novosibirsk, Russian Federation Email: A.A.Kondakov@inp.nsk.su

I. Shikhovtsev

Budker Institute of Nuclear Physics SB RAS Novosibirsk, Russian Federation Email: I.V.Shikhovtsev@inp.nsk.su

V. Amirov

Budker Institute of Nuclear Physics SB RAS

Novosibirsk, Russian Federation Email: V.H.Amirov@inp.nsk.su

D. Gavrisenko

Budker Institute of Nuclear Physics SB RAS Novosibirsk, Russian Federation Email: D.Yu.Gavrisenko@inp.nsk.su

P. Deichuli

Budker Institute of Nuclear Physics SB RAS Novosibirsk, Russian Federation Email: P.P.Deichuli@inp.nsk.su

N. Ilvenko

Budker Institute of Nuclear Physics SB RAS Novosibirsk, Russian Federation Email: N.S.Ilyenko@inp.nsk.su

Abstract

The high-energy neutral injectors based on the acceleration of negative ions (N-NBI) are being developed at the Budker Institute of Nuclear Physics (BINP). The special features of the BINP injector are the RF surface-plasma negative ion source with thermostabilisation of electrodes, the low energy beam transport (LEBT) section between the ion source and accelerator and a wide-aperture multielectrode accelerator, pumped from the both sides. The tank of LEBT section is pumped by cryopumps and it diminishes the entering of gas and impurities to accelerator, while dipole magnets installed in LEBT provide the beam turn to the accelerator entrance. It favors the electrical strength of accelerator and the reliability of the source and injector operation. The accelerated negative ion beam is focused by quadrupole lenses and neutralized by a plasma neutralizer, which provides up to 84% neutralization efficiency for energy negative ions >500 keV. The injector line with 9 A negative ion hydrogen beam production and acceleration to 500 keV for 20 s pulse is planned. The results of negative ion beam production in the 1.5 A source prototype, 1 A beam transport and acceleration to 400 keV at the BINP accelerator teststand as well as the first experiments on a full-scale 9 A negative ion source are presented.

1. INTRODUCTION

The powerful negative ion (NI) based injector for plasma heating in thermonuclear fusion class devices is being developed at the Budker institute of nuclear physics [1]. The injector implements several original approaches in general acceleration scheme and ion source design [2]:

- the negative ion source is separated from the acceleration tube with LEBT section, which purifies the beam and prevents the stray particles and gas from entering the accelerator [3];
- a wide aperture multielectrode accelerator with improved pumping and an increased voltage holding are used [2].

The study of ion beam production, transport and acceleration is carried out on the injector teststand with principal scheme shown in Figure 1.

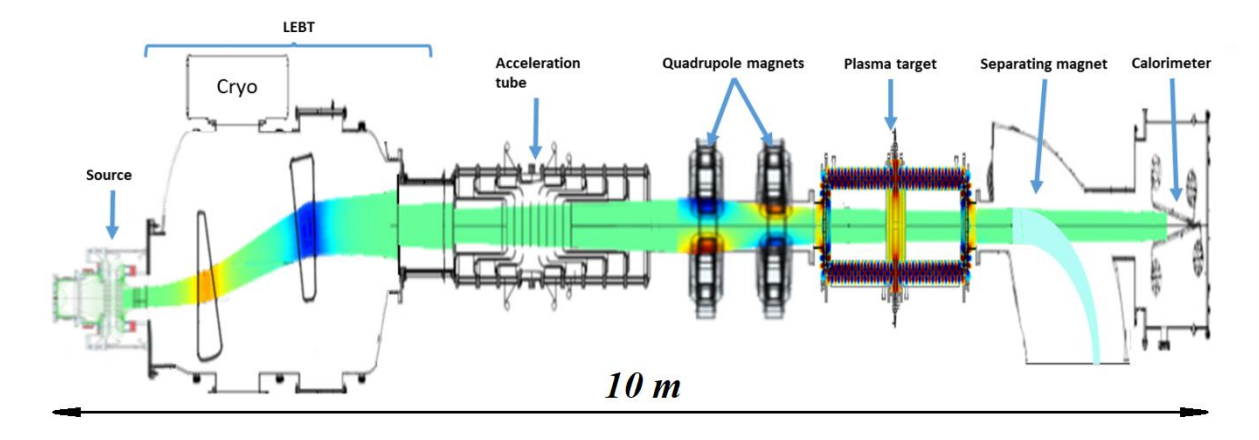


FIG. 1. Scheme of BINP negative ion based neutral beam injector prototype.

The injector teststand is equipped with a 1.5 A prototype ion source and the beam line providing up to 1 A beam transport and acceleration. The 120 keV 1.5 A negative ion prototype source with it power supplies is located on the high voltage platform, biased up to -400 kV potential. The source is attached to the vacuum tank of LEBT section, which is located at the high voltage platform and attached to the accelerating tube. The LEBT tank is equipped with two bending magnets and a high speed cryopumping system. The wide-aperture accelerating tube was designed to accelerate up to 1 A beam and consists of 9 electrodes with entrance aperture of $200 \div 260$ mm. The accelerated beam is focused by quadrupoles and passes to calorimeter.

2. 1.5 A NEGATIVE ION SOURCE

The scheme of the negative ion source [2] is shown in Figure 2. The plasma produced by the RF driver [4] flows through an expansion chamber towards the negative ion converter – to the plasma grid, which is covered by cesium layer to enhance negative ion production. The dipole magnetic filter is used to suppress the electron diffusion and to decrease the electron temperature and density in the region of negative ion production near the plasma grid (PG). Cesium is supplied by heating the external ovens with cesium pellets. Cesium vapour feeds through the heated distribution galleries located at the plasma grid periphery [5]. In order to support the PG optimal cesium coverage and to prevent the cesium accumulation on the extraction grid (EG) both PG and EG were kept hot by circulation of hot thermal liquid through the channels drilled in the electrode bodies.

The positive biasing of plasma grid with respect to the expansion chamber is applied in order to collect the plasma electrons and to reduce the flow of electrons co-extracted together with negative ions. The multiaperture extraction of H⁻ ion in the prototype source is provided with the 21 emission apertures having the internal diameter of 16 mm arranged in a rectangular array on the plasma grid surface with step 27 mm.

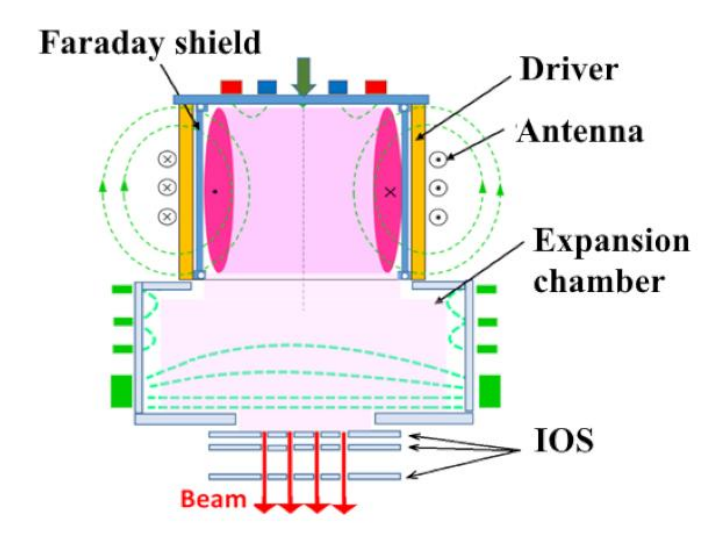


FIG. 2. Scheme of RF negative ion source. Dashed lines -magnetic field of RF antennas and magnetic filter.

The components of inductive 60 kW, 4 MHz RF driver are: 200 mm ceramic tube, a protective Faraday Shield installed inside the ceramic tube to defend it from erosion by plasma. The 3 turn water-cooled antenna made of a copper tube with outer diameter of 6 mm and covered by dielectric sleeve. Back flange is shielded by 2 mm molybdenum disc from the plasma side. Hydrogen is puffed into the discharge chamber with the help of electromagnetic valves, attached to the ignition unit. The RF discharge is initiated by spark plasma from the ignition unit. The RF generator delivers output voltage and power up to 14 kV and 75 kW correspondingly. The RF driver elements and material was optimized to enlarge the driver efficiency [4].

The three-electrodes ion-optical system (IOS) was used to extract and accelerate negative ions from the source. IOS geometry was optimized by the IBSimu code [6]. The IOS extraction gap geometry for one of 21 beamlets of the improved source version is shown in Fig.3. It provides the extraction of the beam with emission current density up to 450 A/m^2 and the interception of the most of co-extracted electrons. The extraction electrode concavity with radius of 1.75 m provides the beam ballistic focusing.

The geometry of acceleration grid apertures were changed in order to decrease beam divergence as well. The accelerating electrode with five 16x124 mm slits was changed to 5x5 array of circular apertures with diameter 16.5 mm. It decreases beam divergence, but reduces IOS pumping and increases beam stripping. The voltages of extraction gap up to 14 kV and of acceleration gap up to 110 kV were applied.

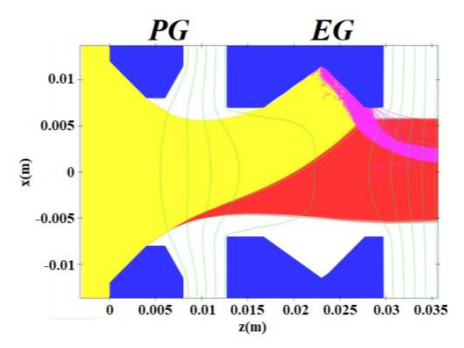


FIG. 3. Beam formation in the extraction gap of the improved source (IBSimu code). Emission aperture internal diameter 16 mm. EG aperture diameter 14 mm, thickness 17 mm. EG voltage 14 kV, H- current density 450 A/m². Red lines - H ions, yellow lines - co-extracted electrons, Magenta lines - trajectories of secondary emitted electrons

The improved prototype source routinely produces the H $^{-}$ beams with a current of 1.2-1.5 A and the energy up to 120 keV in pulses up to 20 s, as it is illustrated in the oscillogram of Figure 4. The 1.5 A, beam production in long pulse 6.5 sec is shown in Figure 4. Track I_b shows the production of 1.5 A 117 keV H $^{-}$ beam in pulse interval 1-7.5 s with the co-extracted electron current value of $I_e = I_{ex} - I_b \sim 1$ A. About 20% growth of coextracted electron current from 0.9 A to 1.1 A was recorded to the pulse end. The growth is probably caused by PG cesium coverage depletion and it could be compensated by addition of cesium [5]. It should be noted that the obtained value of the 1.5 A H $^{-}$ beam at the source exit corresponds to a initial average emission current density of 450 A/m 2 (taking into account 20% stripping of negative ions on the accompanying gas in the IOS).

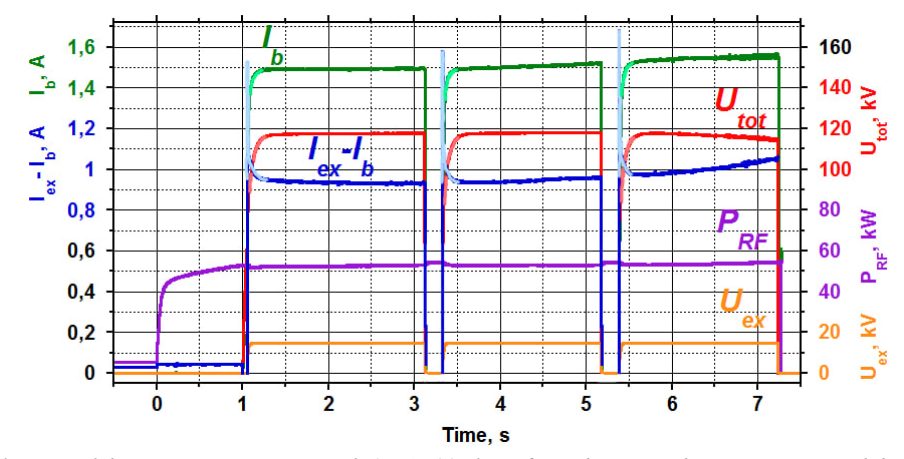


FIG. 4. Oscillogram of the source parameters with 1.5 A, 117 keV, 6 s H beam production. Source with ballistic focusing and circle acceleration grid apertures

The parameters of the beam transported through the LEBT was directly measured by movable Faraday Cup (FC), installed in the LEBT at the distance 2.5 m from the source, and by the secondary emission probes, installed around the LEBT exit aperture. Figure 5 shows the 2-dimensional profile of the 1A, 102 kV beam with the lowest divergence, measured by FC for the beam, produced by the source with the circular apertures of accelerated grid and by concaved extraction grid. As it is seen from Fig.5, the diameter of the beam in the improved source is about 96 mm (FWHM). The lowest beam divergence of ~15 mrad (Fig.5) was recorded at the optimal extraction voltage of 10 kV. The total current, measured by FC with inlet window Ø 170 mm corresponded well with the values, obtained by integration of beam profiles, measured by beam scan with the small collectors Ø10 mm installed behind the openings in main FC plate. Thus IOS scheme have provided an effective beam formation with an emission density of 300 A/m² with lower beam divergence.

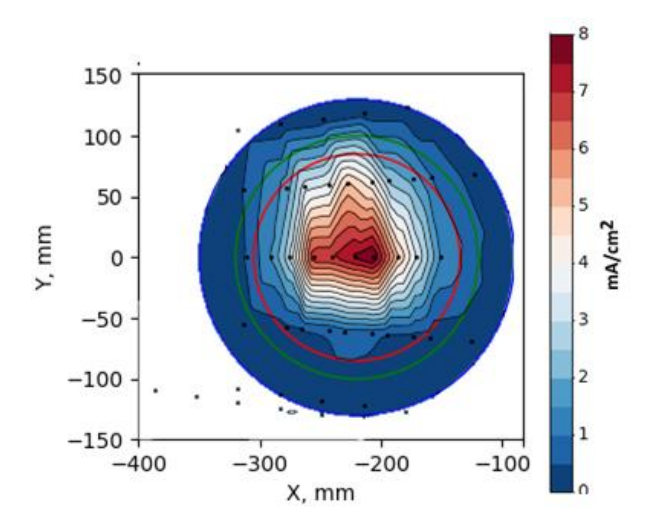


FIG. 5. Beam profile at 2.5 m from the source with ballistic focusing and circle acceleration grid apertures. Probe positions are shown by black dotes. $I_b = 1$ A, $U_b = 120$ keV, $I_{FC} = 0.77$ A, $U_{ex} = 10$ kV

The only cryopump with pumping rate of 10^5 L/sec for hydrogen was used in the case of Fig.6. It provides the residual pressure in the LEBT tank of about $1\cdot10^{-3}$ Pa, so ~ 83% of the beam, outgoing the source was transported to the FC at distance of 2.5 m, and ~ 70% - to the accelerator input at distance 4.5 m.

The effect of the acceleration grid apertures geometry on the profile of the transported beam was calculated by IBSimu code, the code results are illustrated in Figure 6, where the profiles of the beam, transported to the accelerator input for circular and slit geometry of acceleration grid apertures are shown. Beam with 14 mm width (FWHM) was transported to the accelerator input from the source with circular apertures (red profile in Fig.6), while it has 40 mm width (FWHM) in the case of slits apertures (blue profile in Fig.6). In the case of circular apertures more than 90% of the beam could enter through the accelerator input aperture diaphragm with diameter 200mm (see Fig. 7 and Table 1 below).

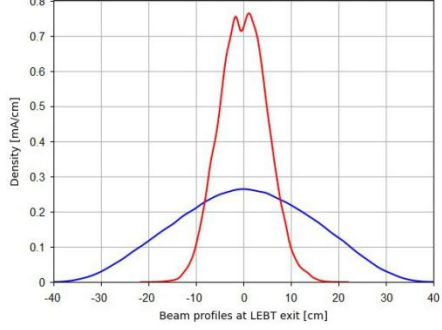


FIG. 6. Beam profiles at LEBT exit (modelling by IBSimu). Blue – acceleration grid with slits, red - with circular apertures. Emission current density $450 \, \text{A/m}^2$.

3. WIDE APERTURE MULTIELECTRODE ACCELERATOR

The H beam acceleration was performed with the wide aperture multielectrode acceleration tube. The cross section of accelerator tube and principal scheme of electrodes connection to power supply are shown in Figure 7. The eight independent rectifiers with voltage up to 60 kV could be connected to acceleration electrode in serial to the eight accelerating gaps. Only six of eight accelerating gaps were powered in the experiments made in 2025, as it is shown in Figure 7. The currents measured in the circuit of the first accelerator electrode (I_P in Figure 7) and the current in the circuit of the last accelerating gaps (I_{HV} in Fig.7) were used to evaluate the beam transmission during acceleration. The directly measured current I_P is the current, entering the accelerator (through the input diaphragm \emptyset 200-240 mm and through the aperture of first electrode of accelerator \emptyset 258 mm). The directly measured current I_{HV} is the current at the accelerator output. It includes the accelerator electrodes. The calculated trajectories of H- ions during acceleration of 120 keV, 1 A beam by applying ~46 kV voltage to each of first six acceleration gaps (with total acceleration voltage 280 kV) are shown in Fig.7 by the red lines. As it is seen from Fig.7, the 120 keV, 1 A beam, entering the accelerator is focused well by the

electrostatic lens, formed by the concave electric field in the first accelerating gap and it provides the 100% beam acceleration to the energy 380~keV for the input window of accelerator with diameter $\sim 240~mm$.

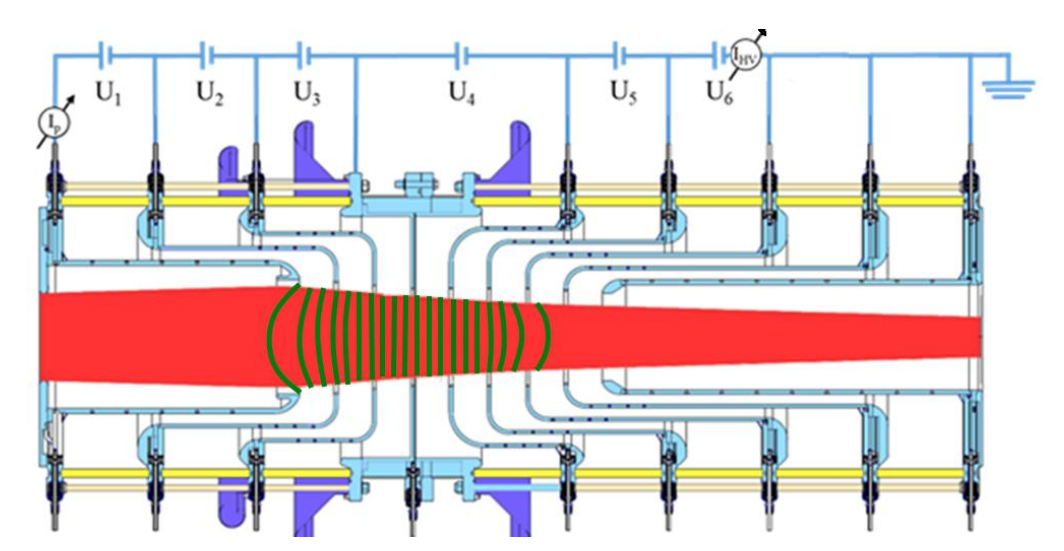


FIG. 5. The acceleration tube cross section and scheme of electrodes powering and currents measurement. Red and green lines – beam trajectories and electric field equipotentials. IBSimu modelling for 120 keV, 1A beam extracted through the 21 apertures. Calculated beamlet divergence at the source exit is 15 mrad.

The currents, measured during 2 s pulse of beam acceleration with HV connection according to scheme of Figure.7 are shown in Figure 8. Green track $I_b \sim 1$ A of Fig.8 is the current, outgoing the source, magenta track $I_p = 0.7\text{-}0.8$ A is the current, entering the accelerator tube, and $I_{HV} = 0.65\text{-}0.75$ A is the current at the accelerator output. Track $U_{HV} = 280$ kV is the total accelerator voltage applied. Gradual ~10-14% growth of beam currents I_p and I_{HV} was recorded to the end of 2 s pulse. Fig.8 illustrates ~ 76% transport of 1 A H $^{\scriptscriptstyle T}$ beam to the accelerator. It is in a good agreement with ~ 24% beam stripping in the LEBT.

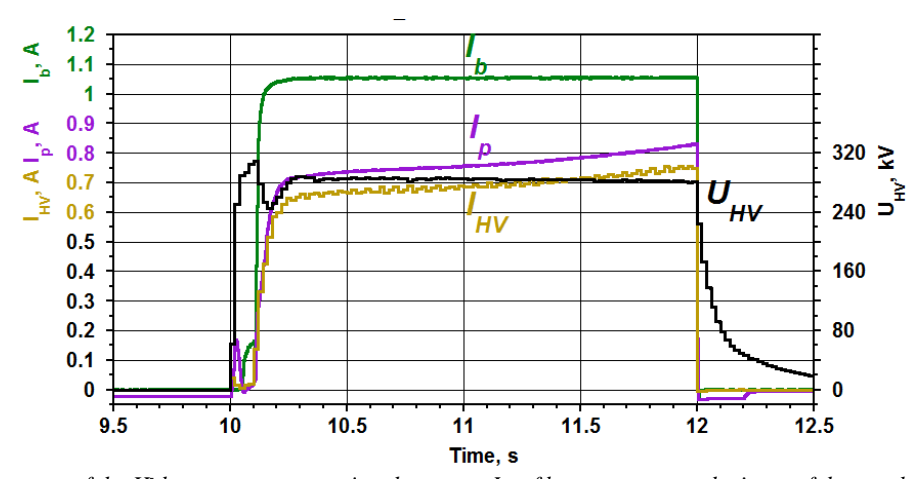


FIG. 6. Oscillograms of the H beam current outgoing the source I_b of beam current at the input of the accelerator I_p and of beam current I_{HV} accelerated to energy 0.4 MeV. U_{HV} – acceleration voltage.

The achieved efficiency I_{HV} / I_p of beam acceleration to energy 400 keV was about 90%. Both values I_{HV} / I_p , I_p / I_b could be increased with correction of beam matching and decreasing beam stripping by better pumping of LEBT and accelerator.

The parameters of the beam formation, efficiencies of the transport and acceleration obtained for various source modifications are summarized in Table 1. The column I_b shows maximum H beam current at the source exit, column I_{ag} shows electron current intercepted by acceleration grid, column "Vacuum" corresponds to LEBT tank vacuum. The next three columns show beam transport efficiency to different z-axis positions: to distances 2.5 m, 3.8 m, and 4.45 m. At z = 2.5 m, the current registered by FC is shown. At the other two positions, there are limiting aperture (LA) with different sizes indicated in brackets. At z = 4.45 m, the current entering

acceleration tube after LA \varnothing 200 or 260 mm is shown, at 4.45 m – the current outgoing accelerator exit aperture \varnothing 200 is shown for LA \varnothing 200 or 260 mm cases.

TABLE 1. BEAM PRODUCTION AND TRANSPORT EFFICIENCY

Acceleration grid apertures	I _b , A (U _{ex} =14 kV)	I _{AG} , A	Vacuum, Pa	I_{FC}/I_b $z = 2.5 \text{ m}$	Accelerator z=4.5 m	
					I_p/I_b	I_{HV}/I_b
Slits 124 mm	1.5	0.68	1•10-3	0.57/1.05 (ø170 FC)	0.6/1.05 (ø260 LA)	0.45/1.05 (ø260 LA)
Circles ø 16.5 mm	1.5	0.75	1•10 ⁻³	0.8/1.05 (ø170 FC)	0.6/1.05 (ø200 LA)	0.6/1.05 (ø200 LA)
	1.5	0.75	0.5•10 ⁻³	_	0.79/1.05 (ø260 LA)	0.75/1.05 (ø260 LA)

All cases, shown in Table 1 were made at the similar RF driver operation parameter. At high extraction voltage beam with I_b =1.5 A was achieved, it doesn't corresponds to optimal beam transport via LEBT. So the extraction voltage of 10 kV provides optimal beam transport efficiency for the beam with current 1 A and energy 100 keV -120 keV. First line shows results for source with slotted acceleration grid. In this case, about 54% of the beam was measured by FC, located at 2.5 m from the source and 57% transmission of the beam to the entrance of acceleration tube through the \varnothing 260 mm diaphragm at 4.45 m was achieved. In the case of source with circle acceleration grid, the FC registered current fraction increases to 76%, and the beam transport efficiency to the distance of 4.45 m is the same – 57%, which corresponds to the decreased acceleration tube diaphragm. The measurements for the last line were done at the higher vacuum pumping speed 2•10⁵ l/s, resulted in decreased beam stripping in LEBT and corresponding beam transport efficiency 75%.

4. 9 A NEGATIVE ION SOURCE

The negative ion source with projected negative ion beam current of 9 A, energy up to 120 keV and pulse duration up to 100 s was designed and manufactured at BINP. The principal scheme of the source is shown in Fig. 9. It includes four RF plasma drivers, an expansion chamber and four-grid IOS with 145 beamlets. Emission apertures Ø 14 mm in the plasma grid are used for beam extraction. Additional pumping is provided at the IOS sides. Thermal stabilization of the IOS grids is provided by circulating a coolant through the internal channels in the grids. A four-channel RF power supply system and HV rectifiers has been manufactured.

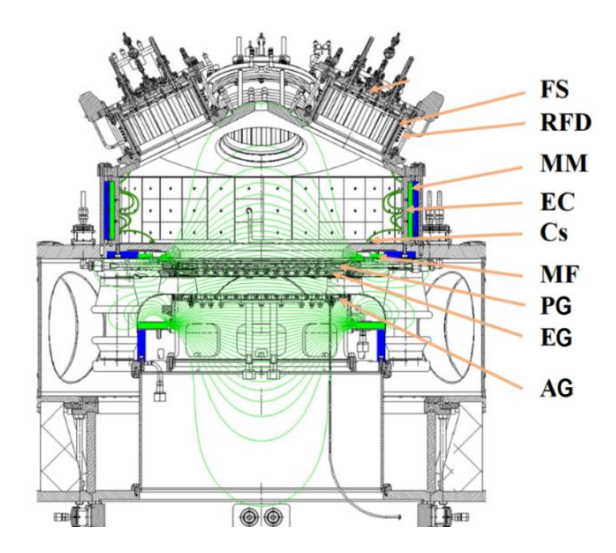


FIG. 7. Cross-section of the source along the magnetic field. The magnetic field lines are shown in green lines. IU-spark ignition of the discharge, RFD-RF driver, FS-Faraday shield, MM-permanent magnets, EC-expansion chamber, Cs- gallery for cesium seed, MF-magnetic filter, PG-plasma grid, EG-extracting grid, AG-accelerating grid.

Tests of a full-scale multi-aperture source with a designed beam current of 9 A has been started on a separate stand. Simultaneous operation of four RF plasma drivers was achieved, and the uniformity of plasma flux entering the plasma electrode was studied using grid probes installed in the plasma grid apertures. The probe's small aperture ø4mm allowed local measuring of plasma characteristics. The ion current density distribution near the plasma electrode, measured using 10 probes is shown in Figure 10. The measurements showed 2-3–fold increase in plasma density in the direction of ExB drift. This plasma heterogeneity should have little effect on the uniformity of the beam production, since H- are mainly formed by the conversion of suprathermal hydrogen atoms formed by the dissociation of hydrogen molecules in the RF driver volume.

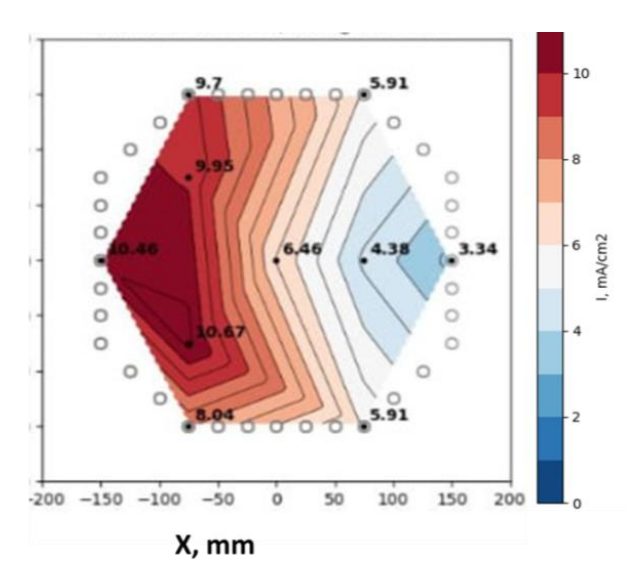


FIG. 8. Plasma positive ion density profile on a plasma grid obtained using a compact plasma grid probes. 4 RF drivers are turned on with total RF power of 120 kW.

5. SUMMARY

The experiments on negative ion beam production, transport and acceleration have been done at the BINP accelerator test stands. The negative ion beam current of about 1.5 A with emission current density of $450 \, \text{A/m}^2$ was obtained in the prototype source. Efficient suppression of co-extracted electron current at the level of about 1 A was demonstrated. 83% of negative ion source current was transported to the 2.5 m distance from the source, 75% of ion source current - through the acceleration tube entrance. $0.65 \div 0.75 \, \text{A}$ beam was accelerated to the energy 0.4 MeV in the pulses with duration 2.5 s. The recorded beam losses are corresponded well to the negative ion stripping on LEBT residual gas.

REFERENCES

- [1] Belchenko Y.I., Burdakov A.V., Davydenko V.I. et al. Possible Scheme of Atomic Beam Injector for Plasma Heating and Current Drive at the TRT Tokamak, Plasma Physics Reports, 47, 1151-1157 (2021)
- [2] O. Sotnikov, A. Ivanov, Yu. Belchenko et al. Development of high-voltage negative ion based neutral beam injector for fusion devices, Nuclear Fusion, 61,116017 (2021)
- [3] A. A. Ivanov; Yu. Belchenko; P. Deichuli et al. Negative ion based neutral injector: Beam formation and transport, AIP Conf. Proc. 1771, 030012 (2016)
- [4] Gavrisenko, D.Y., Shikhovtsev, I.V., Belchenko, Y.I. et al. Comparative analysis of high-frequency plasma drivers with various protective screens for atomic injectors with multi-second pulse duration, Plasma Phys. Rep. 49, 1169 (2023)
- [5] Yu Belchenko, A Ivanov, S Konstantinov et al. Efficient cesiation in RF driven surface plasma negative ion source, Rev. Sci. Instrum. 87, 02B133 (2016)
- [6] T. Kalvas, O. Tarvainen, T. Ropponen; et al. A three-dimensional simulation software for charged particle optics, *Rev. Sci. Instrum.* 81, 02B703 (2010)